JPET Fast Forward. Published on July 29, 2014 as DOI:10.1124/jpet.114.217141

JPET/2014/217141

TITLE: Translational Pharmacokinetic-Pharmacodynamic Modeling for An Orally Available Novel Inhibitor of Anaplastic Lymphoma Kinase and c-Ros Oncogene 1

AUTHORS: Shinji Yamazaki, Justine Lam, Helen Y Zou, Hui Wang, Tod Smeal and Paolo Vicini

ADDRESS: Pharmacokinetics, Dynamics and Metabolism (S.Y., J.L., P.V.) and Oncology Research Unit (H.Y.Z, H.W., T.S.), Pfizer Worldwide Research & Development, San Diego, California

RUNNING TITLE: Translational PKPD Modeling of a Novel ALK Inhibitor

CORRESPONDING AUTHOR:

Shinji Yamazaki, Ph.D.

Pharmacokinetics, Dynamics and Metabolism, La Jolla Laboratories

Pfizer Worldwide Research and Development

10777 Science Center Drive, San Diego, CA 92121, USA

Tel: 858-622-8050 Fax: 858-622-8252

E-mail: shinji.yamazaki@pfizer.com

Number of Text Pages:	37
Number of Tables:	4
Number of Figures:	7
Number of References:	44
Number of Words in the Abstract:	245
Number of Words in the Introduction:	745
Number of Words in the Discussion:	1606

ABBREVIATIONS:

ALK, anaplastic lymphoma kinase; *CL/F*, oral clearance; C_p, plasma concentration; EC_{50}, drug concentration causing 50% of maximum effect; PF06463922, (10*R*)-7-amino-12-fluoro-2,10,16-trimethyl-15-oxo-10,15,16,17-tetrahydro-2*H*-8,4-(metheno)pyrazolo[4,3-*h*][2,5,11]benzoxadiazacyclotetradecine-3-carbonitrile; E_0, ALK phosphorylation baseline; E_{max}, maximum effect; EML4, echinoderm microtubule-associated protein-like 4; k_a, absorption rate constant; KC_{50}, the plasma concentration causing 50% of maximum effect; k_{in}, zero-order formation rate constant, K_{max}, maximal tumor killing rate constant; k_{md}, first-order rate degradation rate constant for a modulator; k_{ng}, net tumor growth rate constant; k_{out} ,first-order degradation rate constant; MET, hepatocyte growth factor receptor; NSCLC, non–small-cell lung cancer; *OFV*, objective function value; PKPD, pharmacokinetic-pharmacodynamic; ROS1, c-Ros oncogene 1; T_{ss}, maximum sustainable tumor volume; *Tsc*, tumor stasis concentration; *V/F*, oral volume of distribution.

ABSTRACT

An orally available macrocyclic small molecule, PF06463922, is a selective inhibitor of anaplastic lymphoma kinase (ALK) and c-Ros oncogene 1 (ROS1). The objectives of the present study were to characterize the pharmacokinetic-pharmacodynamic relationships of PF06463922 between its systemic exposures, pharmacodynamic biomarker (target modulation) and pharmacological response (antitumor efficacy) in athymic mice implanted with H3122 non-small cell lung carcinomas expressing EML4-ALK mutation (EML4-ALK^{L1196M}) and with NIH3T3 cells expressing CD74-ROS1. In these nonclinical tumor models, PF06463922 was orally administered to animals with EML4-ALK^{L1196M} and CD74-ROS1 at twice daily doses of 0.3 to 20 mg/kg/dose and 0.01 to 3 mg/kg/dose, respectively. Plasma concentration-time profiles of PF06463922 were adequately described by a one-compartment pharmacokinetic model. Using the model-simulated plasma concentrations, a pharmacodynamic indirect response model with a modulator sufficiently fit the time-courses of target modulation (i.e., ALK phosphorylation) in tumors of EML4-ALK^{L1196M}-driven models with $EC_{50,in\ vivo}$ of 36 nM free. A drug-disease model based on an indirect response model reasonably fit individual tumor growth curves in both EML4-ALK^{L1196M} and CD74-ROS1-driven models with the estimated tumor stasis concentrations of 51 and 6.2 nM free, respectively. Thus, the $EC_{60,in\ vivo}$ (52 nM free) for ALK inhibition roughly corresponded to the tumor stasis concentration in an EML4-ALK^{L1196M}-driven model, suggesting that 60% ALK inhibition would be required for tumor stasis. Accordingly, we proposed that the $EC_{60,in\ vivo}$ for ALK inhibition corresponding to the tumor stasis could

be considered a minimum target efficacious concentration of PF06463922 for cancer patients in a phase I trial.

INTRODUCTION

Lung cancer has long been one of the most common and lethal malignancies worldwide with 1.8 million new cases and 1.6 million deaths in 2012, representing 13% of new cancers and 19% of cancer mortality (IARC, 2013). The majority of lung cancers (~90%) are non-small cell lung cancers (NSCLC), which consist of a number of subtypes driven by various activated oncogenes (Ettinger et al., 2010; Larsen et al., 2011). Recent advances in molecular profiling technologies have significantly enhanced the development of personalized, molecularly targeted medicines based on individual genetic or protein profiles (Meric-Bernstam et al., 2013; Arnedos et al., 2014). Consequently, molecularly targeted agents for NSCLC patients have become one of the successful personalized cancer therapies (Moreira and Thornton, 2012; Cardarella and Johnson, 2013; Li et al., 2013). For example, the identification of activating epidermal growth factor receptor (EGFR) mutation in NSCLC patients led to the personalized cancer therapy with the first-generation small molecule inhibitors, gefitinib and erlotinib. Unfortunately, clinical responses to these EGFR inhibitors have not been durable in most cancer patients as tumor cells can readily acquire drug resistance by multiple mechanisms such as the secondary mutations in EGFR (e.g., T790M), the amplification of mesenchymal-epithelial transition factor (MET) and the increased activation of the receptor tyrosine kinase, AXL (Chong and Janne, 2013; Remon et al., 2014). Accordingly, the identification of these drug resistance mechanisms led to the development of second-generation inhibitors (Robinson and Sandler, 2013; Yu and Riely, 2013). These principles and practices on personalized cancer therapy have significantly influenced the accelerated approval of the first-generation anaplastic lymphoma kinase

(ALK) inhibitor, crizotinib (Xalkori; PF02341066), by the Food and Drug Administration (FDA) (Gerber and Minna, 2010; Ou, 2012). The FDA approval of crizotinib in 2011 was less than 4 years after ALK rearrangements (e.g., echinoderm microtubule-associated protein-like 4 (EML4)-ALK) in NSCLC patients were first reported (Rikova et al., 2007; Soda et al., 2007). As an example of personalized cancer medicine, the labeling language states that "Xalkori is a kinase inhibitor indicated for the treatment of patients with locally advanced or metastatic NSCLC that is ALK-positive as detected by an FDA-approved test" (FDA, 2014). Unfortunately, as seen with other target therapies such as the first-generation EGFR inhibitors, resistance to crizotinib due to EML4-ALK mutations has been reported even before its approval, leading to the rapid development of second-generation ALK inhibitors for crizotinib-resistant NSCLC patients (Choi et al., 2010; Casaluce et al., 2013; Gridelli et al., 2014).

PF06463922 ((10*R*)-7-amino-12-fluoro-2,10,16-trimethyl-15-oxo-10,15,16,17-tetrahydro-2*H*-8,4-(metheno)pyrazolo[4,3-*h*][2,5,11]benzoxadiazacyclotetradecine-3-carbonitrile) has been identified as an orally available, ATP-competitive selective inhibitor of ALK (including mutations) and c-Ros oncogene 1 (ROS1) (Johnson et al., 2014). PF06463922 is highly potent against ALK phosphorylation in the cell-based assay (H3122 NSCLC cells expressing the EML4-ALK fusion protein) with an IC_{50} of ~2 nM against the wild-type EML4-ALK (without ALK mutations) and ~20 nM against one of the most frequently detected crizotinib-resistant EML4-ALK mutations, EML4-ALK^{L1196M}. Thus, PF06463922 is ~10-fold potent against the wild-type EML4-ALK relative to its most frequently detected mutation (EML4-ALK^{L1196M}), and ~40-fold potent against EML4-ALK^{L1196M} compared to crizotinib with an approximate IC_{50} of ~800 nM.

Moreover, PF06463922 showed significant in vivo inhibition of ALK phosphorylation and antitumor efficacy in an H3122 NSCLC xenograft model with EML4-ALK^{L1196M}, whereas crizotinib failed to exhibit a significant antitumor efficacy in the xenograft model at twice-daily oral doses of 75 mg/kg/dose, which yielded unbound plasma concentrations higher in mice than in patients at clinically recommended twice-daily oral doses of 250 mg (Zou et al., 2014). We previously reported the pharmacokinetic-pharmacodynamic (PKPD) modeling of crizotinib to target modulation and antitumor efficacy driven by the inhibition of ALK (wild-type) and MET phosphorylation in nonclinical tumor models (Yamazaki et al., 2008; Yamazaki et al., 2012; Yamazaki, 2013). PKPD modeling is a powerful mathematical approach linking drug exposures to pharmacodynamic biomarkers and/or pharmacological responses as a function of time, providing a quantitative assessment of in vivo drug potency together with mechanistic insights in drug action (Derendorf et al., 2000; Chien et al., 2005). The objectives of the present study were to characterize PKPD relationships of plasma concentrations of PF06463922 to inhibition of ALK phosphorylation in tumors (target modulation) and antitumor efficacy (pharmacological response) in athymic mice implanted with H3122 NSCLC cells expressing the EML4-ALK^{L1196M}, and together with PKPD relationship to antitumor efficacy in athymic mice implanted with NIH3T3 cells expressing CD74-ROS1. The present PKPD results will be helpful in understanding the PKPD relationships of PF06463922 and also in guiding dose escalation or de-escalation to maintain efficacious exposure in the clinic.

MATERIALS AND METHODS

Chemicals

PF06463922 (chemical purity >99%) and a structurally-related in-house compound (internal standard for analysis) were synthesized by Pfizer Worldwide Research and Development (San Diego, CA) (Johnson et al., 2014). All other reagents and solvents were commercially available and were of either analytical or high performance liquid chromatography grade.

In Vivo PKPD Study

The experimental designs and methods of the in vitro and in vivo PKPD studies were previously reported in part (Zou et al., 2013; Zou et al., 2014). Briefly, three separate repeated oral-dose PKPD studies were conducted with PF06463922 in female athymic nu/nu mice implanted subcutaneously with H3122 NSCLC cells expressing the EML4-ALK^{L1196M} (studies 1 and 2) or NIH3T3 cells expressing CD74-ROS1 (study 3). These nonclinical tumor models with H3122 NSCLC-EML4-ALK^{L1196M} and NIH3T3-CD74-ROS1 are henceforth referred to as ALK- and ROS1-tumor models, respectively. PF06463922 was orally administered to animals twice daily, 7-hour apart, at the doses of 0.3, 1, 3 and 10 mg/kg/dose for 4 days (study 1), 0.3, 1, 3, 10 and 20 mg/kg/dose for 13 days (study 2) and 0.01, 0.03, 0.1, 0.3, 1 and 3 mg/kg/dose for 9 days (study 3). On the last dosing day, a subset of mice was humanely euthanized at 1, 3, 7, 8, 24 and 36 hours after the first daily dose in study 1, at 1, 3, 7, 8 and 24 hours after the first daily dose in study 2, and at 1, 3, 7 and 24 hours after the first daily dose in study 3. Blood samples (n= 3/time point) were collected by exsanguinations via cardiac puncture to determine plasma concentrations of PF06463922. Resected tumors (n= 3/time point)

were snap-frozen and pulverized using liquid nitrogen-cooled cryomortar. Protein lysates were generated, and the level of total phosphorylated ALK protein (ALK phosphorylation) was determined using a capture ELISA method (studies 1 and 2). Tumor volume was measured during the treatment period by electronic Vernier calipers and was calculated as the product of its length × width^2 × 0.4 (studies 2 and 3). Tumor growth inhibition in each treatment group of PF06463922 was calculated as 100 × (1-$\Delta T/\Delta C$), where ΔT and ΔC are the differences in the median tumor volumes between the first and last dosing days in the treatment and vehicle control groups, respectively. Tumor regression was calculated as 100 × ($\Delta T/T_{initial}$), where $T_{initial}$ is the median tumor volume on the first dosing day. All of the procedures were conducted in accordance with the Institute for Laboratory Animal Research Guide for the Care and Use of Laboratory Animals and with Pfizer Animal Care and Use Committee guidelines.

In Vitro Plasma Protein Binding

The free fraction of PF06463922 was determined in mouse plasma at 2 μM (0.8 μg/mL) using the equilibrium dialysis technique as described previously (Yamazaki et al., 2008). Briefly, the study was conducted in a 96-well Teflon® dialysis chamber (HTDialysis LLC, Gales Ferry, CT) using a semi-permeable membrane (Spectra/Por4®, Spectrum, Laguna Hills, CA) with a 12,000-14,000 Da molecular mass cut-off. After the incubation at 37°C for 6 hours, aliquots of plasma and buffer samples were extracted with aliquots of acetonitrile: methanol mixture (1:1, v/v) containing the internal standard and analyzed by a liquid-chromatography tandem mass spectrometry (LC-MS/MS) method as described below. The free fraction in plasma (f_u) was calculated by the following equation:

$$f_u = C_{buffer} / C_{plasma} \qquad (1)$$

where C_{buffer} and C_{plasma} denote the concentrations of PF06463922 in buffer and plasma, respectively, after the incubation.

PF06463922 Analysis

Plasma concentrations of PF06463922 were determined by a LC-MS/MS method after protein precipitation of plasma samples. The LC-MS/MS system consisted of Waters Acquity UPLC system (Waters, Milford, MA) and an API 5500 triple-stage quadrupole mass spectrometer (Applied Biosystems). Both instruments were controlled by Analyst 1.5.2 software (Applied Biosystems). Chromatographic separation of the analytes was achieved using a reverse phase column (Phenomenex Kinetex phenyl-hexyl, 50×2 mm 1.7 µm) at a flow rate of 0.5 mL/min. A binary mobile phase consisted of water with 0.1% formic acid (A) and acetonitrile with 0.1% formic acid (B). The gradient started at 5% B for 0.2 minutes, increased to 95% B over 1.3 minutes, and then held at 95% B for 0.5 minutes. The gradient was returned to the initial condition of 5% B in 0.1 minutes and equilibrated at 5% B for 0.5 minutes before the next injection. The mass spectrometer was operated in the positive ionization mode using multiple reaction monitoring (MRM) at specific precursor ion → product ion transition, *m/z* 407.3→228.0 for PF06463922 and *m/z* 472.3→432.6 for the internal standard. The standard calibration curve was constructed using weighted ($1/\times^2$) linear regression. The calibration curve range was 0.5 to 5000 ng/mL. The back-calculated calibration standard concentrations were within 15% of their theoretical concentrations, with coefficients of variation of less than 15%. The precision and accuracy of the quality control samples were within 15%.

Pharmacokinetic Analysis

A naïve-pooled pharmacokinetic analysis was used to determine pharmacokinetic parameters of PF06463922 in mice. That is, all individual data at each dose were pooled together for pharmacokinetic analysis as if they came from a single individual since plasma concentrations of PF06463922 were available from only a subset of mice (n=3/time points) (Sheiner, 1984). Pharmacokinetic analysis was performed with a standard one-compartment model as implemented in NONMEM® version 7.1.2 (University of California at San Francisco, San Francisco, CA) (Beal and Sheiner, 1992). This model (subroutine ADVAN2 with TRANS2) was parameterized using absorption rate constant (k_a, h^{-1}), oral clearance (*CL/F*, L/h/kg) and oral volume of distribution (*V/F*, L/kg), that were separately determined in each study. Residual variability was characterized by a proportional error model.

PKPD Modeling

Target Modulation: The response of ALK phosphorylation in tumor (expressed as the ratio to vehicle control animal data) to plasma concentrations of PF06463922 was first modeled by an indirect response model. The indirect response model assumed that ALK phosphorylation at baseline was maintained by the balance of formation and degradation rates (Dayneka et al., 1993; Jusko and Ko, 1994). The addition of PF06463922 was considered to inhibit the formation rate, since PF06463922 was a competitive ATP-binding ALK inhibitor. Therefore the following differential equation was used to determine the EC_{50} required for the inhibition of ALK phosphorylation (R):

$$\frac{dR}{dt} = k_{in} \cdot \left(1 - \frac{E_{\max} \times C_p{}^{\gamma}}{EC_{50}{}^{\gamma} + C_p{}^{\gamma}}\right) - k_{out} \cdot R \qquad (1)$$

where k_{in} is the zero-order formation rate constant (h^{-1}), E_{max} is maximum effect, C_p is the plasma concentration of PF06463922 (ng/mL), EC_{50} is the plasma concentration of PF06463922 (ng/mL) causing one-half E_{max}, γ is the Hill coefficient and k_{out} is the first-order degradation rate constant (h^{-1}) of ALK phosphorylation.

Since a rebound of ALK phosphorylation was observed at 24 to 36 h post-dose (i.e., the ALK phosphorylation ratio of greater than unity in the treatment groups relative to the control group), a modulator was incorporated into the indirect response model as a precursor to take account of the observed rebound phenomena, as has been done previously (Sharma et al., 1998). The precursor PKPD model assumed that a modulator (M) was synthesized at a zero-order rate (k_{in}) and degraded at a first-order rate (k_{md}), and an ALK phosphorylation level was maintained by the balance of the first-order formation rate provided by the modulator degradation rate (i.e., k_{md}) and the ALK degradation rate (k_{out}). PF06463922 was considered to inhibit the ALK formation rate, i.e., k_{md}. Accordingly, the following differential equations were used to estimate EC_{50} required for PF06463922-mediated ALK inhibition:

$$\frac{dM}{dt} = k_{in} - k_{md} \cdot \left(1 - \frac{E_{max} \times C_p{}^{\gamma}}{EC_{50}{}^{\gamma} + C_p{}^{\gamma}} \right) \cdot M \qquad (2)$$

$$\frac{dR}{dt} = k_{md} \cdot \left(1 - \frac{E_{max} \times C_p{}^{\gamma}}{EC_{50}{}^{\gamma} + C_p{}^{\gamma}} \right) \cdot M - k_{out} \cdot R \qquad (3)$$

Antitumor Efficacy: Drug-disease modeling for antitumor efficacy to plasma concentration of PF06463922 was performed based on a modified indirect response model (Yamazaki et al., 2008; Wong et al., 2009; Yamazaki et al., 2011). In our approach, a tumor growth model was first established to characterize tumor growth

curves in the vehicle control group. Typical tumor growth curves in nonclinical tumor models are known to follow an exponential growth in the early phases followed by a linear growth, and then eventually reach a plateau phase (Gompertz, 1825; Bissery et al., 1996; Bernard et al., 2012). Accordingly, the individual tumor growth curves in the vehicle control group were first modeled by using a first-order growth rate with and without a logistic function that constrains the maximum tumor volume. An exponential tumor growth model without a logistic function is defined as:

$$\frac{dT}{dt} = k_{ng} \cdot T \qquad (4)$$

where T is tumor volume (mm^3) and k_{ng} is the first-order net growth rate constant (h^{-1}).

In contrast to the exponential tumor growth model, the tumor growth model with a logistic function (logistic tumor growth model) is defined as:

$$\frac{dT}{dt} = k_{ng} \cdot T \cdot \left(1 - T/T_{ss}\right) \qquad (5)$$

where T_{ss} represents the maximum sustainable tumor volume (mm^3), which is assumed to be constant whereas T changes over time.

When T is relatively small in the early stage of tumor growth, the net tumor growth rate is roughly first-order (i.e., exponential growth) since the ratio of T/T_{ss} approximates zero. Thereafter, the net tumor growth rate approaches zero when the T/T_{ss} ratio becomes unity. Thus, the logistic model is applicable if tumor growth starts to slow down in the later stage of tumor growth. In the present study, the logistic model was used in study 2 as the basic tumor growth model whereas the exponential growth model was used in study 3, since each respective model provided a better fit to the individual tumor growth curves (data not shown). The difference in tumor growth function between

these studies could simply reflect tumor growth dynamics which might differ among nonclinical tumor models and individual studies.

Subsequently, the response of tumor volume (*T*) to plasma concentration of PF06463922 (C_p) was modeled based on the assumption that PF06463922 ultimately stimulated the tumor killing rate, thus inhibiting tumor growth rate characterized by either the exponential or logistic tumor growth model:

$$\frac{dT}{dt} = g(T) - \left(\frac{K_{max} \times C_p^{\gamma}}{KC_{50}^{\gamma} + C_p^{\gamma}} \right) \cdot T \qquad (6)$$

where *g(T)* is tumor growth function, K_{max} is the maximal tumor killing rate (h^{-1}) caused by PF06463922, and KC_{50} is the plasma concentration of PF06463922 (ng/mL) causing one-half K_{max}.

Tumor stasis concentration (*Tsc*), defined as the plasma concentration of PF06463922 required to maintain tumor burden constant at steady-state (i.e., 100% tumor growth inhibition meaning zero net tumor growth rate), was calculated using equation 6 above with the obtained pharmacodynamic parameter estimates, assuming zero tumor growth rate, i.e., $dT/dt = 0$ as $C_p = Tsc$

Data Analysis: All PKPD modeling analyses were performed with NONMEM version 7.1.2 with the subroutine ADVAN8. The initial conditions at time zero for the GI tract compartment, ALK phosphorylation ratio and tumor volume were the dose amount (mg/kg), the ALK baseline ratio (i.e., unity) and the measured initial individual tumor volume (mm^3), respectively. Residual variability was characterized by a proportional error model. In the drug-disease model, an inter-animal variability on k_{ng} was estimated by mixed-effect modeling using an exponential variance model and Hill coefficients (γ)

were fixed to be unity. Model selection was based on a number of criteria such as the NONMEM objective function values (*OFVs*), estimates, standard errors, and scientific plausibility, as well as exploratory analysis of standard goodness-of-fit plots. The difference in the *OFVs* between two nested models was compared with a χ^2 distribution in which a difference of 6.63 was considered significant at the 1% level (Wahlby et al., 2001).

RESULTS

Pharmacokinetic Analysis for PF06463922

The increase in plasma concentrations of PF06463922 was roughly dose-proportional at the dose ranges tested in studies 1, 2 and 3. Therefore, pharmacokinetic parameters were estimated together at all doses of each study. Typical pharmacokinetic parameter estimates for *CL/F*, *V/F* and k_a were, respectively, 1.2 L/h/kg, 5.3 L/kg and 2.0 h^{-1} in study 1, 1.1 L/h/kg, 7.0 L/kg and 1.3 h^{-1} in study 2, and 1.7 L/h/kg, 11 L/kg and 4.0 h^{-1} in study 3 (Table 1). These pharmacokinetic parameter estimates with twice-daily doses were comparable to those determined in other studies where the same cumulative dose amounts were delivered with once-daily doses. The standard errors of the majority of estimated pharmacokinetic parameters in studies 1 to 3 were small (CV<30%), with residual variability of 12 to 24%. *OFVs* were 543, 802 and 275 in studies 1, 2 and 3, respectively. A representative example of the observed and one-compartment pharmacokinetic model-fitted plasma concentrations of PF06463922 in study 1 is shown in Fig. 1. Overall, the plasma concentration-time courses of PF06463922 in studies 1, 2 and 3 were adequately described by the one-compartment model. The typical pharmacokinetic parameters thus obtained (i.e., *CL/F*, *V/F* and k_a) were used to simulate plasma concentrations as a function of time following oral administration to drive the pharmacodynamic models.

PKPD Modeling for Target Modulation

The inhibition of ALK phosphorylation was sustained after the first- and second-daily doses and thereafter returned to near or above the baseline at 24 to 36 hour post-dose in studies 1 and 2. In contrast, the plasma concentrations of PF06463922 reached

the maximal levels at 1 hour post-dose and then rapidly declined. The observed and indirect-response model-fitted ALK phosphorylation-time courses along with the simulated plasma concentrations of PF06463922 are graphically presented in Fig. 2. The indirect response model did not fit the ALK inhibition well at 24 to 36 hours post-dose in studies 1 and 2 because the model was unable to account for the ALK rebound. The $EC_{50,in\ vivo}$ was estimated at 137 ng/mL (Table 2). In contrast to the indirect response model, the precursor model fit the time-courses of ALK inhibition sufficiently well, particularly 24 to 36 hour post-dose, yielding the *OFV* value of -284 smaller (i.e., statistically better) than that (-262) from the indirect response model (Fig. 3). The estimated $EC_{50,in\ vivo}$ was 58 ng/mL, which was approximately 2-fold lower than that from the indirect response model. The estimated k_{out} and k_{md} were 1.8 and 0.021 h^{-1}, respectively.

Drug-Disease Modeling for Antitumor Efficacy

In an ALK-tumor model, the observed tumor growth inhibition by PF06463922 was 57, 87, 101, 121 (63% regression) and 120% (66% regression) at the doses of 0.3, 1, 3, 10 and 20 mg/kg/dose, respectively, on the last dosing day (study 2). The model-fitted individual and typical tumor growth inhibition curves with the observed tumor volumes are presented in Fig. 4. The drug-disease model reasonably fit the observed individual tumor growth curves in all groups with an estimated KC_{50} of 33 ng/mL. The estimated k_{max} (0.011 h^{-1}) was 1.1-fold higher than the estimated k_{ng} (0.0094 h^{-1}), indicating that the model-predicted maximal antitumor efficacy was greater than tumor stasis, i.e., tumor regression. The tumor stasis concentration (*Tsc*), which was the plasma concentration of PF06463922 required to maintain tumor stasis at steady-state, was calculated at 83 ng/mL.

In a ROS1-tumor model, the observed tumor growth inhibition by PF06463922 was 26, 38, 84, 104 (20% regression), 116 (73% regression) and 120% (85% regression) at the doses of 0.01, 0.03, 0.1, 0.3, 1 and 3 mg/kg/dose, respectively, on the last dosing day (study 3). The model-fitted individual and typical tumor growth inhibition curves with the observed tumor volumes are presented in Fig. 5. The drug-disease model sufficiently fit the observed tumor volumes in all groups. Estimated k_{max} (0.020 h^{-1}) was 2.3-fold higher than the estimated k_{ng} (0.0086 h^{-1}), indicating that the model-predicted maximal antitumor efficacy was a significant tumor regression. The estimated KC_{50} was 13 ng/mL, which was nearly comparable to the calculated *Tsc* of 10 ng/mL.

Quantitative Comparison of PKPD Relationships

The concentration-response curves of ALK inhibition and tumor growth inhibition based on the obtained pharmacodynamic parameters (e.g., $EC_{50,in\ vivo}$ and E_{max}) from ALK- and ROS1-tumor models are graphically presented in Fig. 6. It may be worth noting that the tumor growth inhibition ranges from 0 to 120% while the range of ALK inhibition is 0 to 100% in Fig. 6. Based on the calculation method for tumor growth inhibition (%) as indicated in Materials and Methods, the maximum tumor growth inhibition was near 110% even though the estimated k_{max} (0.020 h^{-1}) was approximately 2-fold higher than the estimated k_{ng} (0.0086 h^{-1}) in a ROS1-tumor model. In an ALK-tumor model, the $EC_{50,in\ vivo}$ (58 ng/mL) for ALK inhibition was 1.4-fold lower than the estimated *Tsc* (83 ng/mL). Thus, the *Tsc* was roughly comparable to the $EC_{60,in\ vivo}$ (85 ng/mL) for ALK inhibition. The $EC_{60,in\ vivo}$ estimate for ALK inhibition and *Tsc* as total plasma concentrations (bound plus unbound) were corresponding to 52 and 51 nM free, respectively, with the correction for an unbound fraction of 0.25 in mouse plasma

(Table 4). The estimated *Tsc* (10 ng/mL corresponding to 6.2 nM free) in a ROS1-tumor model was approximately 10-fold lower than that (51 nM free) in an ALK-tumor model, demonstrating that PF06463922-mediated antitumor efficacy was more potent in a ROS1-tumor models than an ALK-tumor model as consistent with the difference in the $EC_{50,in\ vitro}$ values of 0.2 and 15 nM for ROS1 and ALK inhibition, respectively.

DISCUSSION

In the present study, we quantified the relationships of plasma concentrations of PF06463922 to inhibition of ALK phosphorylation and tumor growth inhibition in a crizotinib-resistant ALK-tumor model (i.e., H3122 NSCLC with EML4-ALK^{L1196M}) using a mathematical modeling approach. This is the first report to quantitatively characterize PKPD relationships of a second generation ALK inhibitor for target modulation (including rebounds) and antitumor efficacy in an ALK-tumor model. Unexpectedly, the rebounds of ALK phosphorylation in vivo were observed at 24 to 36 hours after repeated oral administration of PF06463922. By that time, the plasma concentrations of PF06463922 declined to less than 5 ng/mL (3 nM free), which was >10-fold lower than the $EC_{50,in\ vivo}$ (36 nM free). The observations that ALK responses were partially back to near or above the baseline around 24 h post-dose were consistent in an ALK-tumor model treated with not only PF06463922, but also other in-house ALK inhibitors. Moreover, the degree of ALK rebound was more pronounced in study 2 (day 13) than study 1 (day 4). That is, the ALK phosphorylation ratios at 24 h post-dose after 13-day repeated administration were higher than those after 4-day repeated administration, suggesting that ALK rebounds increased with the length of dosing period. Accordingly, in order to describe the available data and estimate $EC_{50,in\ vivo}$, it was critical to incorporate a modulator into an indirect response model to take account of the time-dependent ALK responses including rebound phenomena. Since the biological mechanism for ALK rebounds in an ALK-tumor model is still unclear, we have applied several previously proposed feedback and precursor PKPD models to the present results in addition to an indirect response model (Gabrielsson and Weiner, 2000). None of these

PKPD models except for a precursor model could acceptably fit the time-course of ALK responses. The $EC_{50,in\ vivo}$ (58 ng/mL) estimated by the precursor model was >2-fold lower than that (137 ng/mL) with an indirect response model, suggesting accounting for the ALK rebounds would be important to estimate pharmacodynamic parameters.

It has been known that adaptive resistance to molecularly target agents (e.g., tyrosine kinase inhibitors) can occur immediately in cancer patients through a rapid wiring of cancer cell signaling (Soria et al., 2012; Rosell et al., 2013). There are also limited data suggesting that a signaling rebound may occur after the cessation of cancer therapy with tyrosine kinase inhibitors in patients who develop drug-resistance (Riely et al., 2007). Thus, the network signals can possibly and quickly undergo adaptive changes during cancer therapy with tyrosine kinase inhibitors. It has also been reported that changes in total receptor abundance could affect tyrosine kinase inhibitor-mediated target modulation, when it was measured as amount of phosphorylated protein corrected for total protein (Kirouac et al., 2013). Some ATP-competitive tyrosine kinase inhibitors such as crizotinib could affect an interaction between the HSP90 charperone and its client kinases, resulting in changes of kinase stabilization (Taipale et al., 2013). The biological feedback mechanisms, including the observed ALK rebounds in vivo, might be one of the potential reasons for the 2-fold difference in the estimated $EC_{50,in\ vivo}$ between in vivo (36 nM free) and in vitro (15 nM free) (Table 4), although the 2-fold difference could be within the expected variability derived from in vitro and in vivo experiments. It would be worth noting that significant antitumor efficacy of PF06463922 was consistently observed throughout the treatment period in an ALK-tumor model we studied, despite the ALK responses being partially back to near or above the baseline prior to each dose. For

example, the ALK phosphorylation ratios at 24 h post-dose were near baseline on day 4 and approximately 2 on day 13 at the dose of 3 mg/kg/dose twice daily whereas tumor growth inhibition at this dose was consistently near-tumor stasis during the treatment period with 98% tumor growth inhibition on day 13. Therefore, the ALK rebounds in nonclinical models may not be related to antitumor resistance to ALK inhibitors.

Regarding the PKPD relationship of target modulation to antitumor efficacy, the $EC_{60,in\ vivo}$ (52 nM free) for ALK inhibition was comparable to the estimated *Tsc* (51 nM free) in an ALK-tumor model (Table 4). This relationship suggested that >60% ALK inhibition would be required for tumor stasis. We previously developed an integrated PKPD model to comprehensively characterize relationships between inhibitor concentrations, biomarker responses and antitumor efficacy (Yamazaki et al., 2011; Yamazaki, 2013). In the integrated model, pharmacodynamic parameters obtained by the PKPD model were used to simulate biomarker responses as a function of time to model antitumor efficacy using a proposed "inhibition index" (1/*E*-1) as the variable driving the effect. However, in the present study, the inhibition index became negative when ALK rebounds were observed (i.e., E >1), resulting in a predicted increase in model-simulated tumor growth rate which was not supported by our observations. Therefore, we did not apply the integrated model to the present study. In a previous nonclinical study (Yamazaki et al., 2012), the PKPD relationship of crizotinib-mediated ALK inhibition to antitumor efficacy in an H3122 NSCLC model with wild type EML4-ALK (without ALK mutations) was characterized by a similar PKPD modeling approach, where a link model was applied to estimate crizotinib-mediated ALK inhibition. One of the potential reasons for the difference in PKPD models applied between crizotinib and PF06463922 could be

their difference in tumor distribution. That is, crizotinib extensively distributed into tumors of nonclinical models with an approximate tumor/plasma area under the concentration-time curve ratio of 4 at steady-state, whereas the distribution of PF06463922 into tumor was less extensive with the approximate tumor/plasma ratio being close to unity. Differently from the present study with PF06463922, 50% ALK inhibition by crizotinib ($EC_{50,in\ vivo}$ = 19 nM free) was associated with 50% tumor growth inhibition (EC_{50} = 20 nM free) in the previous studies (Yamazaki et al., 2012). Thus, PF06463922-mediated ALK inhibition in an ALK-tumor model (with ALK mutation) appeared to lead to more pronounced antitumor efficacy than crizotinib-mediated ALK inhibition in an H3122 NSCLC model with wild-type EML4-ALK. In a previously reported crizotinib PKPD simulation in patients using clinically observed pharmacokinetic parameters (Yamazaki, 2013), the predicted crizotinib-mediated ALK inhibition could reach 75% at steady-state in patients at the clinically recommended doses of 250 mg twice daily. Collectively, the $EC_{75,vivo}$ (100 nM free) for PF06463922-mediated ALK inhibition could be considered a target plasma concentration for crizotinib-resistant NSCLC patients to achieve crizotinib-equivalent antitumor efficacy as was observed in crizotinib-sensitive NSCLC patients with wild-type ALK rearrangements (Kwak et al., 2010; Camidge et al., 2012). Furthermore, the $EC_{60,in\ vivo}$ (52 nM free) could be considered as a minimum target efficacious concentration in NSCLC patients with EML4-ALK mutations, since tumor stasis was achieved with 60% ALK inhibition in an ALK-tumor model.

In a ROS1-tumor model, we could not determine $EC_{50,in\ vivo}$ for ROS1 inhibition because of a lack of specificity of the ROS1 antibody, whereas the decrease in the

numbers of Ki67 positive cells in tumor cells was confirmed with as an anti-proliferation marker with an immune-histochemistry analysis(Zou et al., 2013). The $EC_{50,in\ vitro}$ estimate (0.2 nM free) for ROS1 inhibition was >50-fold lower than that for ALK inhibition while the *Tsc* estimate in a ROS1-tumor model was approximately 10-fold lower than that in an ALK-tumor model (Table 4). One might expect more pronounced antitumor efficacy by PF06463922 in a ROS1-tumor model, but antitumor potency could result from its target modulation through complex biological mechanisms. For example, the previous crizotinib reports suggested that >50% ALK inhibition corresponded to >50% tumor growth inhibition in an H3122 NSCLC model as discussed above, whereas >90% MET inhibition was required for the same degree of tumor growth inhibition in a GTL16 gastric cancer model (Yamazaki et al., 2008; Yamazaki et al., 2012; Yamazaki, 2013). Recent emerging systems pharmacology approaches also suggest the view of an extensive and intricate signaling cross-talk and scaffold networks within cancer cells during tumorigenesis and tumor progression (Rikova et al., 2007; Guo et al., 2008; Kirouac et al., 2013). When the $EC_{50,in\ vitro}$ (0.2 nM) for ROS1 inhibition was compared to the observed plasma concentration of PF06463922 in a ROS1-tumor model, the average plasma concentration (0.5 nM free) at the lowest dose of 0.01 mg/kg was approximately 3-fold higher than the $EC_{50,in\ vitro}$. However, the observed antitumor efficacy at this dose level was minimal with tumor growth inhibition of 26% on the last dosing day, suggesting that the $EC_{50,in\ vivo}$ for ROS1 inhibition could be higher than the $EC_{50,in\ vitro}$ to achieve an antitumor efficacy comparable to that observed in an ALK-tumor model. Nevertheless, the comparison of PF06463922-mediated antitumor efficacy between ROS1 and ALK suggested that antitumor efficacy in cancer patients with ROS1

rearrangements would be achieved more readily. Therefore, we could expect a significant antitumor efficacy of PF06463922 in patients with ROS1 rearrangements when its systemic exposure reached a proposed targeted efficacious concentration based on ALK inhibition.

In conclusion, the PKPD relationships among systemic exposures of PF06463922, target modulation and antitumor efficacy in nonclinical tumor models were characterized well in a quantitative manner using a mathematical modeling approach (Fig. 7). The present modeling efforts suggest that >60% ALK inhibition would be required for tumor stasis in an ALK-tumor model. Accordingly, we proposed that the $EC_{60,in\ vivo}$ for ALK inhibition (~50 nM free) could be considered a minimum target efficacious concentration of PF06463922 in NSCLC patients with EML4-ALK rearrangements (with and without ALK mutations). The proposed minimum efficacious concentration could also be enough to lead to a significant antitumor efficacy in patients with ROS1 rearrangements. Overall we believe that the present PKPD results will be helpful in understanding clinical PKPD relationships of PF06463922 and also in guiding dose escalation or de-escalation to maintain efficacious exposure to PF06463922 in the clinic.

ACKNOWLEDGMENT

We greatly acknowledge members of Pharmacokinetics, Dynamics and Metabolism department (Pfizer Worldwide Research and Development, Groton, CT), especially, Amanda King-Ahmad, Andre Negahban, Jian Lin, Beijing Tan and Yizhong Zhang for the in vitro studies and bioanalytical analyses, and Dac Dinh, Lars Engstrom, Hieu Lam, Nathan Lee, Qiuhua Li, Ruth W Tang, Sergei Timofeevski, Konstantinos Tsaparikos and Melissa West (Oncology Research Unit, Pfizer Worldwide Research and Development, San Diego, CA) and Hovhannes Gukasyan (La Jolla Research Support, Pfizer Worldwide Research and Development, San Diego, CA) for the in vivo studies and pharmacodynamic analyses. We also thank Bhasker Shetty and Bill Smith (Pharmacokinetics, Dynamics and Metabolism, Pfizer Worldwide Research & Development, San Diego, CA) for excellent inputs of the draft manuscript.

AUTHORSHIP CONTRIBUTION

Participated in research design: Lam, Smeal, Wang, Yamazaki and Zou

Conduct experiments: Wang and Zou

Contributed new reagents or analytic tools: na

Performed data analysis: Lam, Vicini, Yamazaki and Zou

Wrote or contribute to the writing of the manuscript: Lam, Smeal, Vicini, Wang, Yamazaki and Zou

REFERENCES

Arnedos M, Vielh P, Soria JC and Andre F (2014) The genetic complexity of common cancers and the promise of personalized medicine: is there any hope? *J Pathol* **232**:274-282.

Beal S and Sheiner L (1992) NONMEM user guides. *NONMEM project group*:University of California at San Francisco, San Francisco, CA.

Bernard A, Kimko H, Mital D and Poggesi I (2012) Mathematical modeling of tumor growth and tumor growth inhibition in oncology drug development. *Expert Opin Drug Metab Toxicol* **8**:1057-1069.

Bissery MC, Vrignaud P, Lavelle F and Chabot GG (1996) Experimental antitumor activity and pharmacokinetics of the camptothecin analog irinotecan (CPT-11) in mice. *Anticancer Drugs* **7**:437-460.

Camidge DR, Bang YJ, Kwak EL, Iafrate AJ, Varella-Garcia M, Fox SB, Riely GJ, Solomon B, Ou SH, Kim DW, Salgia R, Fidias P, Engelman JA, Gandhi L, Janne PA, Costa DB, Shapiro GI, Lorusso P, Ruffner K, Stephenson P, Tang Y, Wilner K, Clark JW and Shaw AT (2012) Activity and safety of crizotinib in patients with ALK-positive non-small-cell lung cancer: updated results from a phase 1 study. *The lancet oncology* **13**:1011-1019.

Cardarella S and Johnson BE (2013) The impact of genomic changes on treatment of lung cancer. *Am J Respir Crit Care Med* **188**:770-775.

Casaluce F, Sgambato A, Maione P, Rossi A, Ferrara C, Napolitano A, Palazzolo G, Ciardiello F and Gridelli C (2013) ALK inhibitors: a new targeted therapy in the treatment of advanced NSCLC. *Target Oncol* **8**:55-67.

Chien JY, Friedrich S, Heathman MA, de Alwis DP and Sinha V (2005) Pharmacokinetics/Pharmacodynamics and the stages of drug development: role of modeling and simulation. *Aaps J* **7**:E544-559.

Choi YL, Soda M, Yamashita Y, Ueno T, Takashima J, Nakajima T, Yatabe Y, Takeuchi K, Hamada T, Haruta H, Ishikawa Y, Kimura H, Mitsudomi T, Tanio Y and Mano H (2010) EML4-ALK mutations in lung cancer that confer resistance to ALK inhibitors. *The New England journal of medicine* **363**:1734-1739.

Chong CR and Janne PA (2013) The quest to overcome resistance to EGFR-targeted therapies in cancer. *Nat Med* **19**:1389-1400.

Dayneka NL, Garg V and Jusko WJ (1993) Comparison of four basic models of indirect pharmacodynamic responses. *Journal of pharmacokinetics and biopharmaceutics* **21**:457-478.

Derendorf H, Lesko LJ, Chaikin P, Colburn WA, Lee P, Miller R, Powell R, Rhodes G, Stanski D and Venitz J (2000) Pharmacokinetic/pharmacodynamic modeling in drug research and development. *J Clin Pharmacol* **40**:1399-1418.

Ettinger DS, Akerley W, Bepler G, Blum MG, Chang A, Cheney RT, Chirieac LR, D'Amico TA, Demmy TL, Ganti AK, Govindan R, Grannis FW, Jr., Jahan T, Jahanzeb M, Johnson DH, Kessinger A, Komaki R, Kong FM, Kris MG, Krug LM, Le QT, Lennes IT, Martins R, O'Malley J, Osarogiagbon RU, Otterson GA, Patel JD, Pisters KM, Reckamp K, Riely GJ, Rohren E, Simon GR, Swanson SJ, Wood DE and Yang SC (2010) Non-small cell lung cancer. *J Natl Compr Canc Netw* **8**:740-801.

FDA (2014) Xalkori prescribing information. *Available at http://wwwaccessdatafdagov/drugsatfda_docs/label/2011/202570s000lblpdf*

Gabrielsson J and Weiner D (2000) Pharmacokinetic and Pharmacodynamic Data Analysis: Concepts and Applications. *3rd ed, Swedish Pharmaceutical Press, Stockholm, Sweden*.

Gerber DE and Minna JD (2010) ALK inhibition for non-small cell lung cancer: from discovery to therapy in record time. *Cancer Cell* **18**:548-551.

Gompertz B (1825) On the nature of the function expressive of the law of human mortality, and on the new mode of determining the value of life contingencies. *Phil Trans R Soc Lond* **115**:513-585.

Gridelli C, Peters S, Sgambato A, Casaluce F, Adjei AA and Ciardiello F (2014) ALK inhibitors in the treatment of advanced NSCLC. *Cancer Treat Rev* **40**:300-306.

Guo A, Villen J, Kornhauser J, Lee KA, Stokes MP, Rikova K, Possemato A, Nardone J, Innocenti G, Wetzel R, Wang Y, MacNeill J, Mitchell J, Gygi SP, Rush J, Polakiewicz RD and Comb MJ (2008) Signaling networks assembled by oncogenic EGFR and c-Met. *Proc Natl Acad Sci U S A* **105**:692-697.

IARC (2013) GLOBOCAN 2012: Estimated Cancer Incidence, Mortality and Prevalence Worldwide in 2012. http://globocan.iarc.fr/Default.aspx. *International Agency for Research on Cancer (IARC), World Health Organization (WHO)*.

Johnson TW, Richardson PF, Bailey S, Brooun A, Burke BJ, Collins MR, Cui JJ, Deal JG, Deng YL, Dinh D, Engstrom LD, He M, Hoffman J, Hoffman RL, Huang Q, Kania RS, Kath JC, Lam H, Lam JL, Le PT, Lingardo L, Liu W, McTigue M, Palmer CL, Sach NW, Smeal T, Smith GL, Stewart AE, Timofeevski S, Zhu H, Zhu J, Zou HY and Edwards MP (2014) Discovery of PF-06463922, a macrocyclic inhibitor of ALK/ROS1 with pre-clinical brain availability and broad spectrum potency against ALK-resistant mutations. *Journal of Medicinal Chemistry (submitted)*.

Jusko WJ and Ko HC (1994) Physiologic indirect response models characterize diverse types of pharmacodynamic effects. *Clin Pharmacol Ther* **56**:406-419.

Kirouac DC, Du JY, Lahdenranta J, Overland R, Yarar D, Paragas V, Pace E, McDonagh CF, Nielsen UB and Onsum MD (2013) Computational modeling of ERBB2-amplified breast cancer identifies combined ErbB2/3 blockade as superior to the combination of MEK and AKT inhibitors. *Science signaling* **6**:ra68.

Kwak EL, Bang YJ, Camidge DR, Shaw AT, Solomon B, Maki RG, Ou SH, Dezube BJ, Janne PA, Costa DB, Varella-Garcia M, Kim WH, Lynch TJ, Fidias P, Stubbs H, Engelman JA, Sequist LV, Tan W, Gandhi L, Mino-Kenudson M, Wei GC, Shreeve SM, Ratain MJ, Settleman J, Christensen JG, Haber DA, Wilner K, Salgia R, Shapiro GI, Clark JW and Iafrate AJ (2010) Anaplastic lymphoma kinase inhibition in non-small-cell lung cancer. *The New England journal of medicine* **363**:1693-1703.

Larsen JE, Cascone T, Gerber DE, Heymach JV and Minna JD (2011) Targeted therapies for lung cancer: clinical experience and novel agents. *Cancer J* **17**:512-527.

Li T, Kung HJ, Mack PC and Gandara DR (2013) Genotyping and genomic profiling of non-small-cell lung cancer: implications for current and future therapies. *J Clin Oncol* **31**:1039-1049.

Meric-Bernstam F, Farhangfar C, Mendelsohn J and Mills GB (2013) Building a personalized medicine infrastructure at a major cancer center. *J Clin Oncol* **31**:1849-1857.

Moreira AL and Thornton RH (2012) Personalized medicine for non-small-cell lung cancer: implications of recent advances in tissue acquisition for molecular and histologic testing. *Clin Lung Cancer* **13**:334-339.

Ou SH (2012) Crizotinib: a drug that crystallizes a unique molecular subset of non-small-cell lung cancer. *Expert Rev Anticancer Ther* **12**:151-162.

Remon J, Moran T, Majem M, Reguart N, Dalmau E, Marquez-Medina D and Lianes P (2014) Acquired resistance to epidermal growth factor receptor tyrosine kinase inhibitors in EGFR-mutant non-small cell lung cancer: a new era begins. *Cancer Treat Rev* **40**:93-101.

Riely GJ, Kris MG, Zhao B, Akhurst T, Milton DT, Moore E, Tyson L, Pao W, Rizvi NA, Schwartz LH and Miller VA (2007) Prospective assessment of discontinuation and reinitiation of erlotinib or gefitinib in patients with acquired resistance to erlotinib or gefitinib followed by the addition of everolimus. *Clin Cancer Res* **13**:5150-5155.

Rikova K, Guo A, Zeng Q, Possemato A, Yu J, Haack H, Nardone J, Lee K, Reeves C, Li Y, Hu Y, Tan Z, Stokes M, Sullivan L, Mitchell J, Wetzel R, Macneill J, Ren JM, Yuan J, Bakalarski CE, Villen J, Kornhauser JM, Smith B, Li D, Zhou X, Gygi SP, Gu TL, Polakiewicz RD, Rush J and Comb MJ (2007) Global survey of phosphotyrosine signaling identifies oncogenic kinases in lung cancer. *Cell* **131**:1190-1203.

Robinson KW and Sandler AB (2013) EGFR tyrosine kinase inhibitors: difference in efficacy and resistance. *Curr Oncol Rep* **15**:396-404.

Rosell R, Karachaliou N, Morales-Espinosa D, Costa C, Molina MA, Sansano I, Gasco A, Viteri S, Massuti B, Wei J, Cao MG and Bueno AM (2013) Adaptive resistance to targeted therapies in cancer. *Translational lung cancer research* **2**:152-159.

Sharma A, Ebling WF and Jusko WJ (1998) Precursor-dependent indirect pharmacodynamic response model for tolerance and rebound phenomena. *J Pharm Sci* **87**:1577-1584.

Sheiner LB (1984) The population approach to pharmacokinetic data analysis: rationale and standard data analysis methods. *Drug Metab Rev* **15**:153-171.

Soda M, Choi YL, Enomoto M, Takada S, Yamashita Y, Ishikawa S, Fujiwara S, Watanabe H, Kurashina K, Hatanaka H, Bando M, Ohno S, Ishikawa Y, Aburatani H, Niki T, Sohara Y, Sugiyama Y and Mano H (2007) Identification of the transforming EML4-ALK fusion gene in non-small-cell lung cancer. *Nature* **448**:561-566.

Soria JC, Mok TS, Cappuzzo F and Janne PA (2012) EGFR-mutated oncogene-addicted non-small cell lung cancer: current trends and future prospects. *Cancer Treat Rev* **38**:416-430.

Taipale M, Krykbaeva I, Whitesell L, Santagata S, Zhang J, Liu Q, Gray NS and Lindquist S (2013) Chaperones as thermodynamic sensors of drug-target interactions reveal kinase inhibitor specificities in living cells. *Nature Biotechnology* **31**:630.

Wahlby U, Jonsson EN and Karlsson MO (2001) Assessment of actual significance levels for covariate effects in NONMEM. *J Pharmacokinet Pharmacodyn* **28**:231-252.

Wong H, Belvin M, Herter S, Hoeflich KP, Murray LJ, Wong L and Choo EF (2009) Pharmacodynamics of 2-[4-[(1E)-1-(hydroxyimino)-2,3-dihydro-1H-inden-5-yl]-3-(pyridine-4-yl)-1H-pyraz ol-1-yl]ethan-1-ol (GDC-0879), a potent and selective B-Raf kinase inhibitor: understanding relationships between systemic concentrations, phosphorylated mitogen-activated protein kinase kinase 1 inhibition, and efficacy. *J Pharmacol Exp Ther* **329**:360-367.

Yamazaki S (2013) Translational pharmacokinetic-pharmacodynamic modeling from nonclinical to clinical development: a case study of anticancer drug, crizotinib. *Aaps J* **15**:354-366.

Yamazaki S, Nguyen L, Vekich S, Shen Z, Yin MJ, Mehta PP, Kung PP and Vicini P (2011) Pharmacokinetic-pharmacodynamic modeling of biomarker response and tumor growth inhibition to an orally available heat shock protein 90 inhibitor in a human tumor xenograft mouse model. *J Pharmacol Exp Ther* **338**:964-973.

Yamazaki S, Skaptason J, Romero D, Lee JH, Zou HY, Christensen JG, Koup JR, Smith BJ and Koudriakova T (2008) Pharmacokinetic-pharmacodynamic modeling of biomarker response and tumor growth inhibition to an orally available cMet kinase inhibitor in human tumor xenograft mouse models. *Drug Metab Dispos* **36**:1267-1274.

Yamazaki S, Vicini P, Shen Z, Zou HY, Lee J, Li Q, Christensen JG, Smith BJ and Shetty B (2012) Pharmacokinetic/pharmacodynamic modeling of crizotinib for anaplastic lymphoma kinase inhibition and antitumor efficacy in human tumor xenograft mouse models. *J Pharmacol Exp Ther* **340**:549-557.

Yu HA and Riely GJ (2013) Second-generation epidermal growth factor receptor tyrosine kinase inhibitors in lung cancers. *J Natl Compr Canc Netw* **11**:161-169.

Zou HY, Engstrom L, Li Q, Lu MW, Tang RW, Wang H, Timofeevski S, Lam J, Yamazaki S, Hu W, Gukasyan H, Lee N, Johnson TW, Fantin V and Smeal T (2013) PF-06463922, a novel ROS1/ALK inhibitor, demonstrates sub-nanomolar potency against oncogenic ROS1 fusions and capable of blocking the resistant ROS1G2032R mutant in preclinical tumor models. *at the AACR Annual Meeting 2013, Washington, DC, April 2013, American Associations for Cancer Research*

Zou HY, Engstrom LD, Li Q, West M, Tang RW, Wang H, Tsaparikos K, Wang J, Timofeevski S, Dinh DM, Lam H, Lam JL, Yamazaki S, Hu W, Affolter T, Lappin PB, Gukasyan H, Lee N, Deng S, Johnson TW, Fantin VR and Smeal T (2014) PF-06463922, a novel next generation ALK/ROS1 inhibitor overcomes both acquired and pharmacological resistance to crizotinib in pre-clinical models. *Nature Medcine (submitted).*

FOOTNOTES

Send reprint requests to: Shinji Yamazaki, Ph.D., Pharmacokinetics, Dynamics and Metabolism, La Jolla Laboratories, Pfizer Worldwide Research and Development, 10777 Science Center Drive, San Diego, CA 92121.

E-mail: shinji.yamazaki@pfizer.com

LEGENDS FOR FIGURES

Fig. 1. Observed and model-fitted plasma concentrations of PF06463922 in athymic mice implanted with H3122 NSCLC cells expressing the EML4-ALK^{L1196M} following repeated oral administration. PF06463922 was orally administered to animals (n = 3 per time point) at the doses of 0.3 to 10 mg/kg/dose twice daily, 7-hour apart, for 4 days. The x-axis represents the time after dosing in hours and the y-axis represents the observed plasma concentrations of PF06463922 (OBS) with the model-fitted individual (IPRED) and typical (PRED) profiles in nanograms per milliliter on a logarithmic scale in study 1

Fig. 2. Indirect response model-fitted and observed ALK inhibition by PF06463922 in athymic mice implanted with H3122 NSCLC cells expressing the EML4-ALK^{L1196M} following repeated oral administration. PF06463922 was orally administered to animals (n = 3 per time point) twice daily, 7-hour apart, at the doses of 0.3 to 10 mg/kg/dose for 4 days in study 1 (S1) and 0.3 to 20 mg/kg for 13 days in study 2 (S2). The x-axis represents the time after the last dosing in hours, the left side of the y-axis represents the observed (ALK OBS) and model-fitted (ALK PRED) ALK inhibition in the ratio to the mean value of control animal data, and the right side of y-axis represents the model-fitted plasma concentrations of PF06463922 (CP PRED) in nanograms per milliliter on a logarithmic scale.

Fig. 3. Precursor model-fitted and observed ALK inhibition by PF06463922 in athymic mice implanted with H3122 NSCLC cells expressing the EML4-ALK^{L1196M}

following repeated oral administration. PF06463922 was orally administered to animals (n = 3 per time point) twice daily, 7-hour apart, at the doses of 0.3 to 10 mg/kg/dose for 4 days in study 1 (S1) and 0.3 to 20 mg/kg for 13 days in study 2 (S2). The x-axis represents the time after the last dosing in hours, the left side of the y-axis represents the observed (ALK OBS) and model-fitted (ALK PRED) ALK inhibition in the ratio to the mean value of control animal data, and the right side of y-axis represents the model-fitted plasma concentrations of PF06463922 (CP PRED) in nanograms per milliliter on a logarithmic scale.

Fig. 4. Observed tumor volumes and model-fitted tumor growth inhibition curves in athymic mice implanted with H3122 NSCLC cells expressing the EML4-ALK^{L1196M} following repeated oral administration of PF06463922. Animals (n = 15 per group) were orally received PF06463922 twice daily, 7-hour apart, at the doses of 0.3 to 20 mg/kg for 13 days (study 2). The x-axis represents the treatment period in days and the y-axis represents the observed individual tumor volumes (OBS) with the model-fitted individual (IPRED) (A) and typical (PRED) (B) tumor growth curves in cubic millimeters.

Fig. 5. Observed tumor volumes and model-fitted tumor growth inhibition curves in athymic mice implanted with NIH3T3 cells expressing the CD74-ROS1 following repeated oral administration of PF06463922. Animals (n = 12 per group) were orally received PF06463922 twice daily, 7-hour apart, at the doses of 0.01 to 3 mg/kg for 9 days (study 3). The x-axis represents the treatment period in days and the y-axis represents the

observed individual tumor volumes (OBS) with the model-fitted individual (IPRED) (A) and typical (PRED) (B) tumor growth curves in cubic millimeters.

Fig. 6. Comparison of PF06463922 concentration-response curves for target modulation and tumor growth inhibition in nonclinical tumor models.

Concentration-response curves for ALK inhibition and tumor growth inhibition were simulated at the concentration range of 0.01 to 10000 ng/mL using the pharmacodynamic parameters estimated from nonclinical tumor models with H3122 NSCLC cells expressing the EML4-ALK^{L1196M} (A) and NIH3T3 cells expressing the CD74-ROS1 (B). Red dashed lines indicate the estimated tumor stasis concentration (*Tsc*), the EC_{60} estimate for ALK inhibition (EC_{60}) and the proposed minimum target efficacious concentration (C_{eff}). The x-axis represents the plasma concentrations of PF06463922 in nanograms per milliliter on a logarithmic scale, the left y-axis represents tumor growth inhibition as percent inhibition and the right y-axis represents ALK inhibition as percent inhibition.

Fig. 7. PKPD modeling summary of target modulation and antitumor efficacy by PF06463922 in nonclinical tumor models.

D, dose; k_a, absorption rate constant (h^{-1}); C_p, plasma concentration (ng/mL); *V*, volume of distribution (L/kg); k_{el}, elimination rate constant (h^{-1}); *M*, modulator; k_{in}, zero-order formation rate constant for a modulator (h^{-1}), k_{md}, first-order degradation rate constant for a modulator and formation rate constant for ALK (h^{-1}); E_{max}, maximum effect; EC_{50}, plasma concentration causing one-half E_{max} (ng/mL); γ, Hill coefficient; *E*, ALK response

(ratio to baseline); k_{out} , first-order degradation rate constant for ALK (h^{-1}); *T*, tumor volume (mm^3); *g(T)*, tumor growth function; K_{max}, maximal tumor killing rate (h^{-1}); KC_{50}, plasma concentration causing one-half K_{max} (ng/mL); k_{ng}, first-order net growth rate constant (h^{-1}); T_{ss}, maximum sustainable tumor volume (mm^3).

TABLE 1

Pharmacokinetic parameter estimates of PF06463922 in nonclinical tumor models following twice daily oral administration

Study	Dose	*CL/F*	*V/F*	k_a	*OFV*
	mg/kg	*L/h/kg*	*L/kg*	h^{-1}	
1	0.3 − 10	1.2	5.3	2.0	543
		(0.1)	(0.8)	(0.6)	
2	0.3 − 20	1.1	7.0	1.3	802
		(0.2)	(0.9)	(0.1)	
3	0.01 − 3	1.7	11	4.0	275
		(0.1)	(1)	(2.2)	

Precision of the estimates is expressed as S.E. in parentheses.

TABLE 2

Pharmacodynamic parameter estimates of PF06463922 for ALK phosphorylation in nonclinical tumor models following twice daily repeated oral administration

Model	EC_{50}	E_0	E_{max}	k_{out}	k_{md}	γ	*OFV*
	ng/mL			h^{-1}	h^{-1}		
IDR	137	1	1	4.8	na	0.95	-262
	(18)	(fixed)	(fixed)	(1.7)		(0.08)	
PCS	58	1	1	1.8	0.021	1.1	-284
	(14)	(fixed)	(fixed)	(0.4)	(0.003)	(0.1)	

Precision of the estimates is expressed as S.E. in parentheses.

IDR, indirect response model; PCS, precursor model; na, not applicable.

TABLE 3

Pharmacodynamic parameter estimates of PF06463922 for tumor growth inhibition in nonclinical tumor models following twice daily repeated oral administration

Study	KC_{50}	K_{max}	k_{ng}	T_{ss}	γ	OFV
	ng/mL	h^{-1}	h^{-1}	mm^3		
2	33	0.011	0.0094	1530	1	5376
	(14)	(0.001)	(0.0012)	(201)	(fixed)	
3	13	0.020	0.0086	–	1	3976
	(3)	(0.001)	(0.0008)		(fixed)	

Precision of the estimates is expressed as S.E. in parentheses.

–, not available.

TABLE 4

Summary of pharmacodynamic parameter estimates for ALK inhibition and antitumor efficacy by PF06463922 in two different nonclinical tumor models

Nonclinical Model	Target Modulation				Antitumor Efficacy
	$EC_{50,vitro}$[a]	$EC_{50,in\ vivo}$	$EC_{60,in\ vivo}$	$EC_{75,vivo}$	*Tsc*
	nM free	*nM free*	*nM free*	*nM free*	*nM free*
H3122-EML4-ALK^{L1196M}	15	36	52	100	51
NIH3T3-CD74-ROS1	0.2	–	–	–	6.2

[a] The values are cited from the previous reports (Zou et al., 2013; Zou et al., 2014). –, not available.

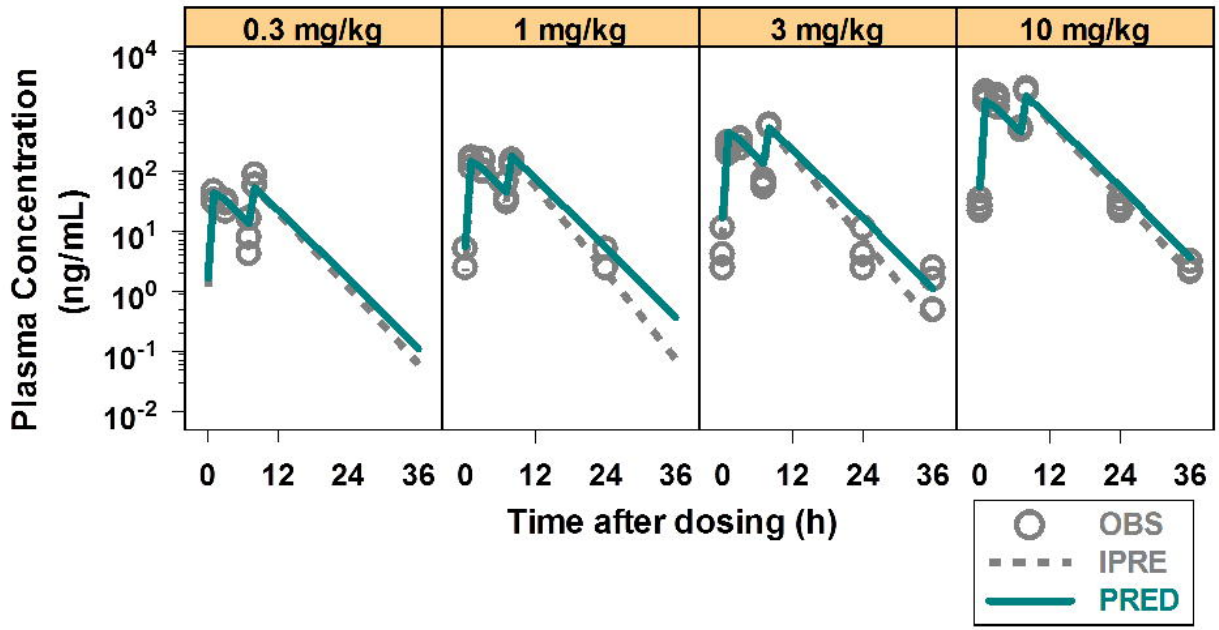
0.3 mg/kg
1 mg/kg
3 mg/kg
10 mg/kg
Plasma Concentration (ng/mL)
10^4
10^3
10^2
10^1
10^0
10^{-1}
10^{-2}
0
12
24
36
Time after dosing (h)
OBS
IPRE
PRED

Figure 1

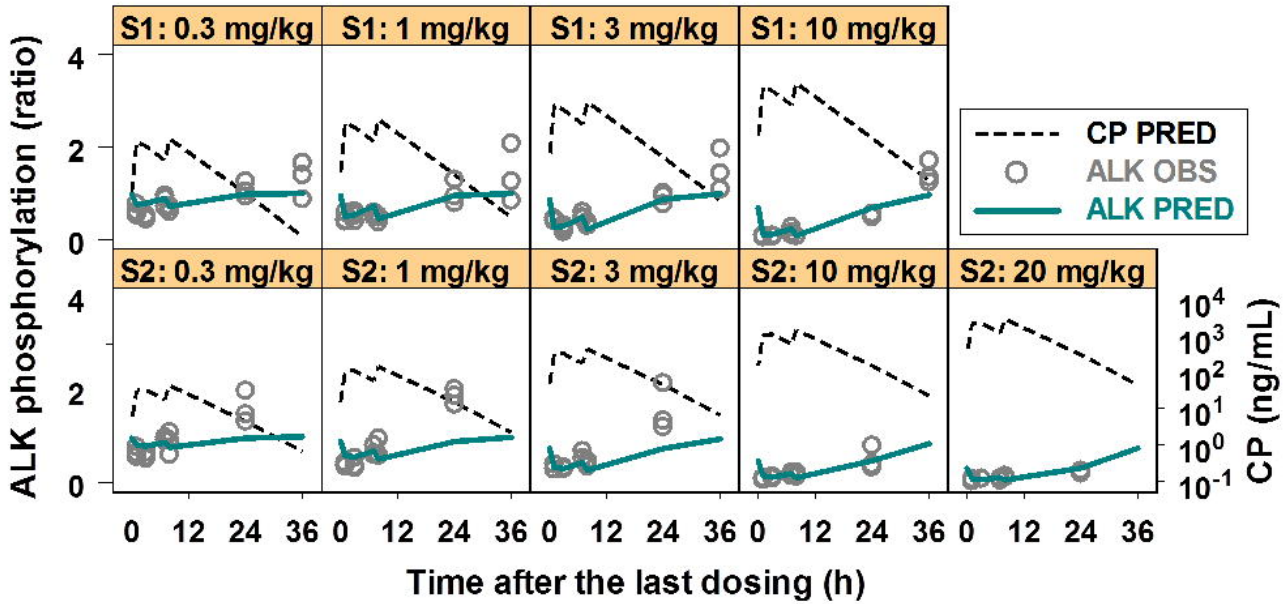
S1: 0.3 mg/kg
S1: 1 mg/kg
S1: 3 mg/kg
S1: 10 mg/kg
S2: 0.3 mg/kg
S2: 1 mg/kg
S2: 3 mg/kg
S2: 10 mg/kg
S2: 20 mg/kg
CP PRED
ALK OBS
ALK PRED
ALK phosphorylation (ratio)
CP (ng/mL)
Time after the last dosing (h)
0
2
4
12
24
36
10^{-1}
10^{0}
10^{1}
10^{2}
10^{3}
10^{4}

Figure 2

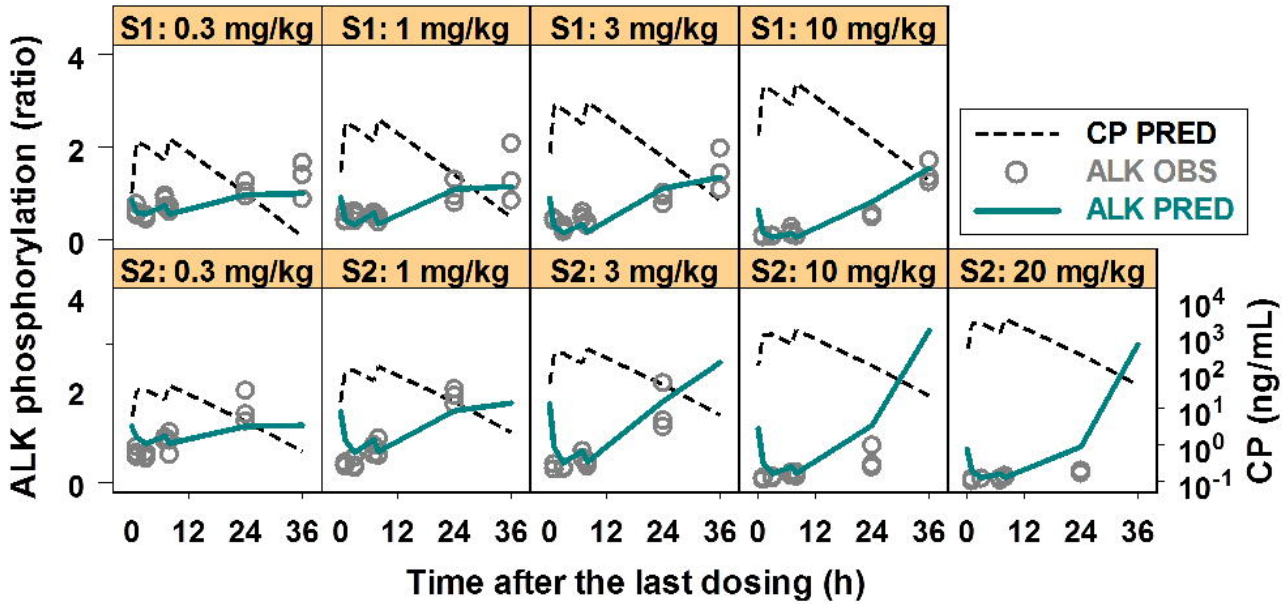
S1: 0.3 mg/kg
S1: 1 mg/kg
S1: 3 mg/kg
S1: 10 mg/kg
S2: 0.3 mg/kg
S2: 1 mg/kg
S2: 3 mg/kg
S2: 10 mg/kg
S2: 20 mg/kg
CP PRED
ALK OBS
ALK PRED
ALK phosphorylation (ratio)
CP (ng/mL)
Time after the last dosing (h)
0
2
4
12
24
36
10^{-1}
10^{0}
10^{1}
10^{2}
10^{3}
10^{4}

Figure 3

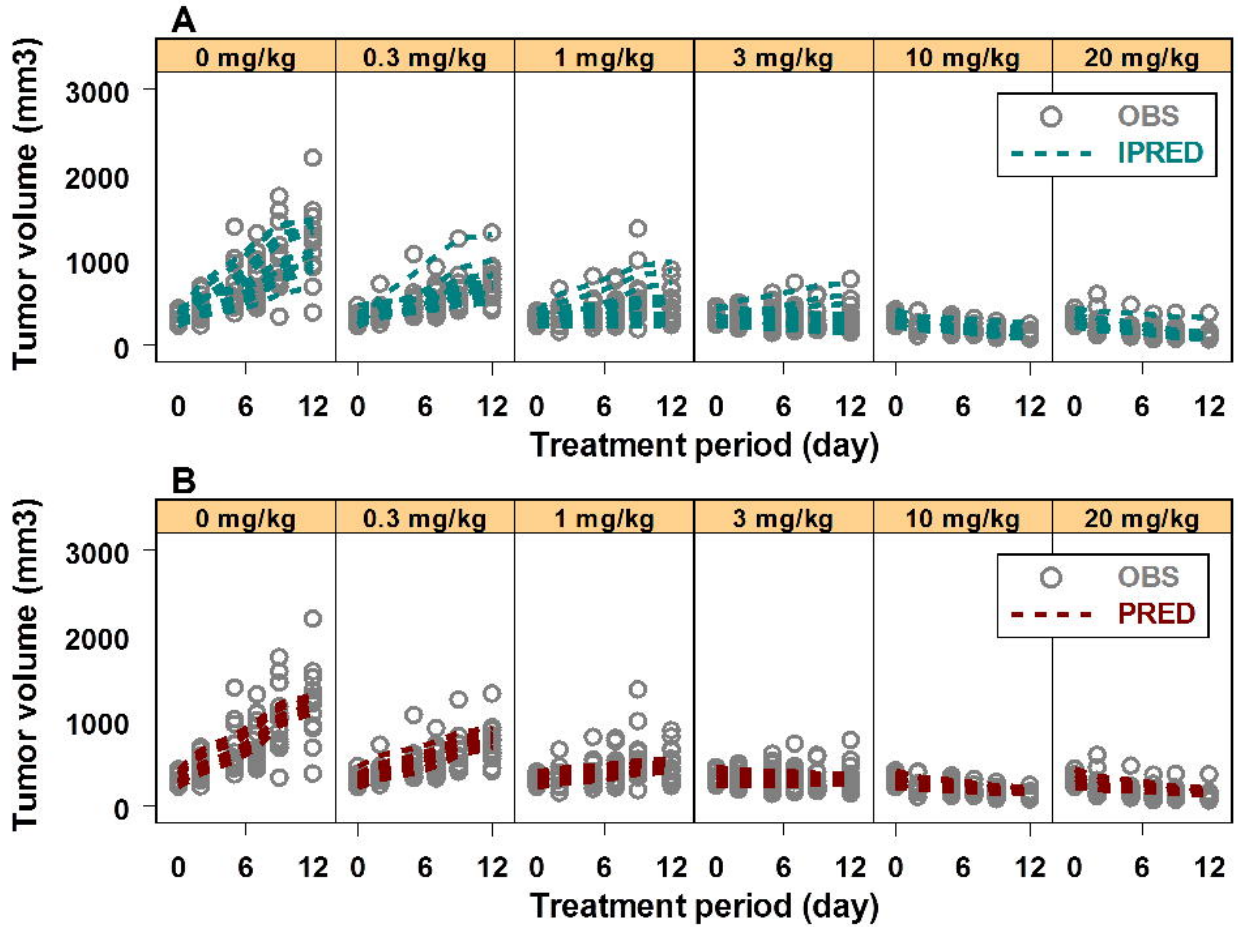
A
0 mg/kg
0.3 mg/kg
1 mg/kg
3 mg/kg
10 mg/kg
20 mg/kg
Tumor volume (mm3)
3000
2000
1000
0
OBS
IPRED
0
6
12
Treatment period (day)
B
0 mg/kg
0.3 mg/kg
1 mg/kg
3 mg/kg
10 mg/kg
20 mg/kg
Tumor volume (mm3)
3000
2000
1000
0
OBS
PRED
0
6
12
Treatment period (day)

Figure 4

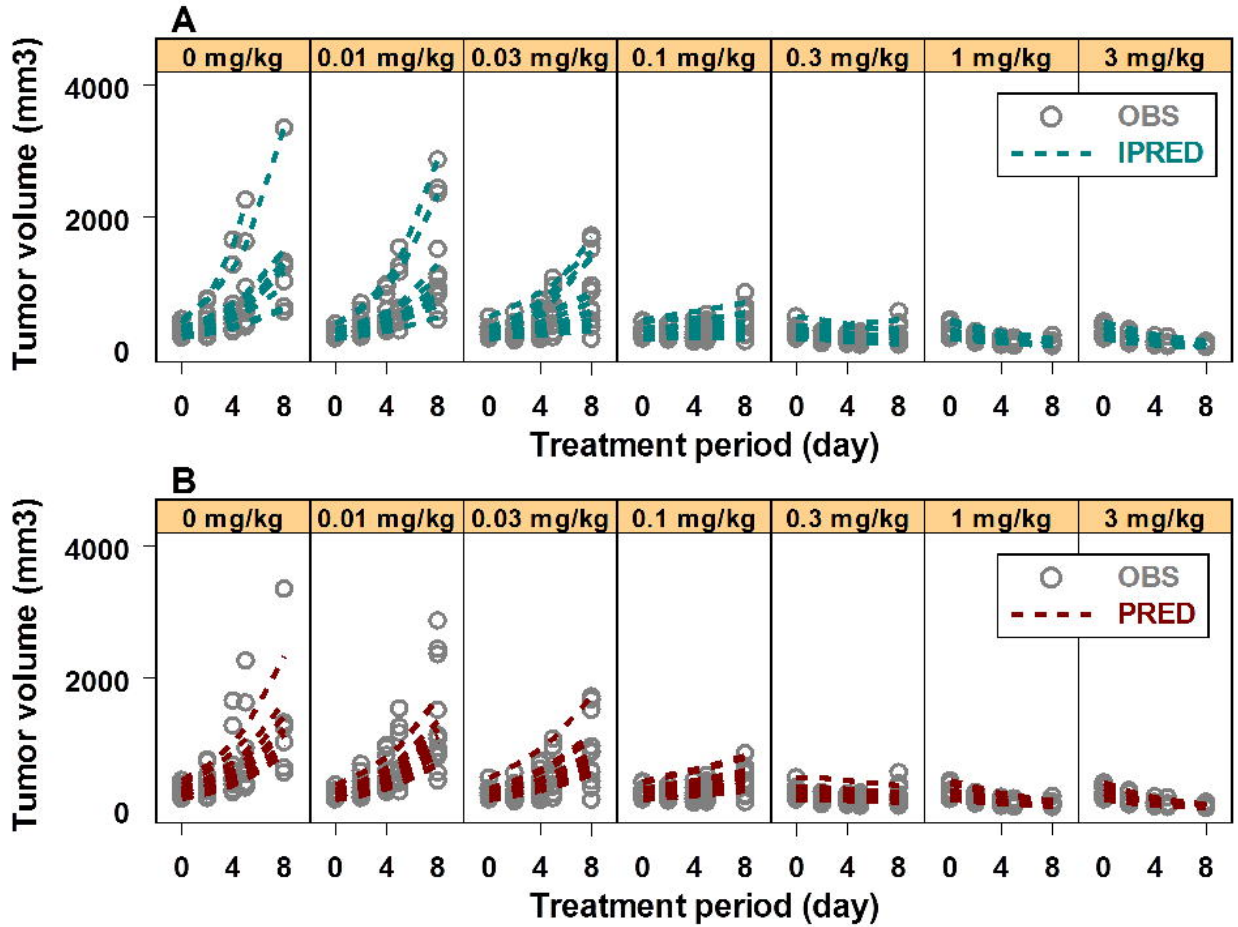
A
0 mg/kg
0.01 mg/kg
0.03 mg/kg
0.1 mg/kg
0.3 mg/kg
1 mg/kg
3 mg/kg
Tumor volume (mm3)
4000
2000
0
OBS
IPRED
0 4 8
Treatment period (day)
B
0 mg/kg
0.01 mg/kg
0.03 mg/kg
0.1 mg/kg
0.3 mg/kg
1 mg/kg
3 mg/kg
Tumor volume (mm3)
4000
2000
0
OBS
PRED
0 4 8
Treatment period (day)

Figure 5

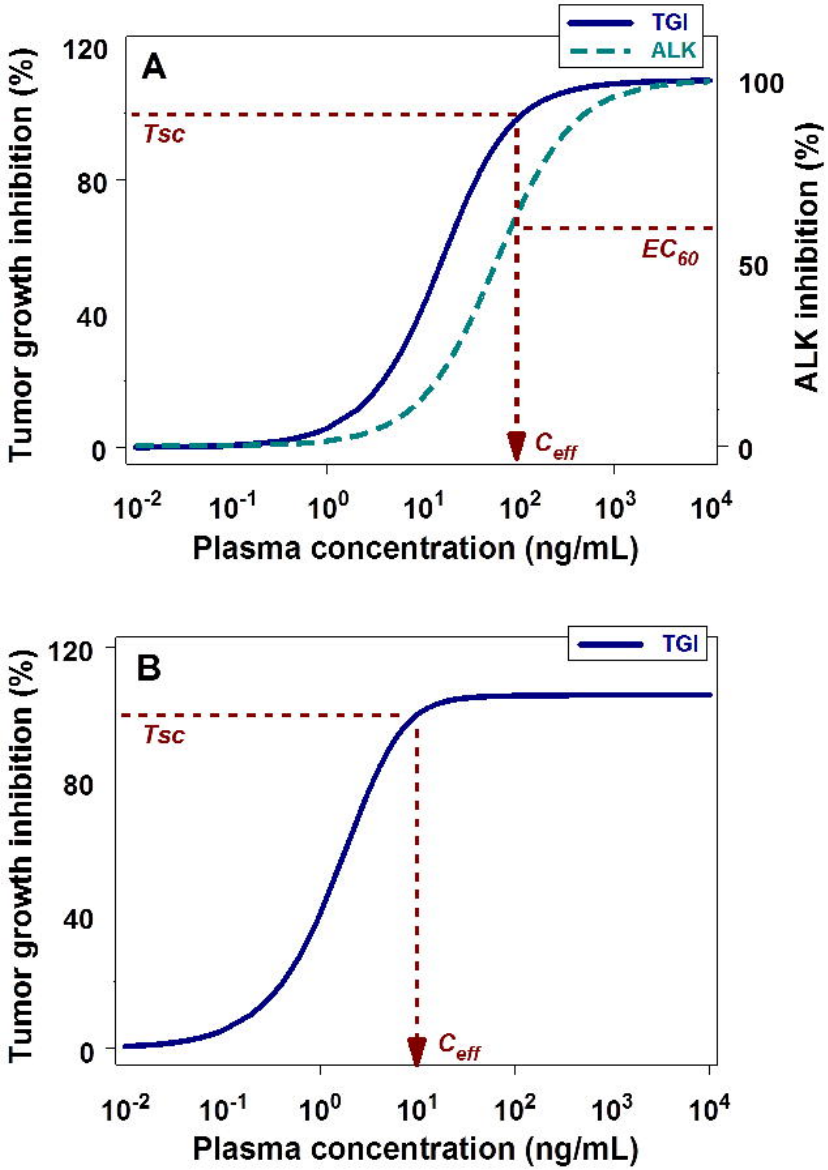
A
TGI
ALK
Tsc
EC60
Ceff
Tumor growth inhibition (%)
ALK inhibition (%)
120
80
40
0
100
50
0
10-2
10-1
100
101
102
103
104
Plasma concentration (ng/mL)
B
TGI
Tsc
Ceff
Tumor growth inhibition (%)
120
80
40
0
10-2
10-1
100
101
102
103
104
Plasma concentration (ng/mL)

Figure 6

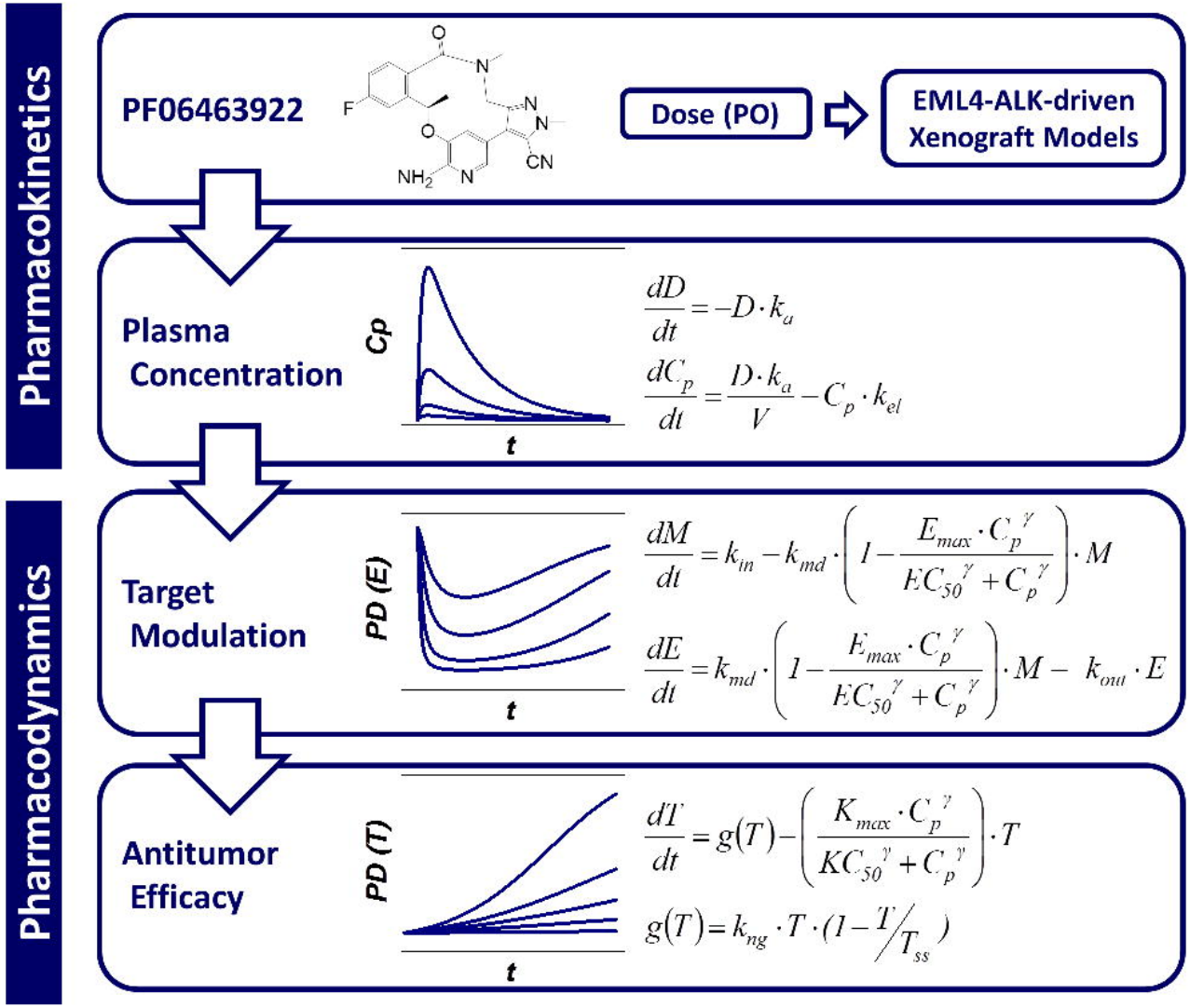
Pharmacokinetics
PF06463922
Dose (PO)
EML4-ALK-driven Xenograft Models
Plasma Concentration
Cp
t
$\frac{dD}{dt} = -D \cdot k_a$
$\frac{dC_p}{dt} = \frac{D \cdot k_a}{V} - C_p \cdot k_{el}$
Pharmacodynamics
Target Modulation
PD (E)
t
$\frac{dM}{dt} = k_{in} - k_{md} \cdot \left(1 - \frac{E_{max} \cdot C_p^{\gamma}}{EC_{50}^{\gamma} + C_p^{\gamma}}\right) \cdot M$
$\frac{dE}{dt} = k_{md} \cdot \left(1 - \frac{E_{max} \cdot C_p^{\gamma}}{EC_{50}^{\gamma} + C_p^{\gamma}}\right) \cdot M - k_{out} \cdot E$
Antitumor Efficacy
PD (T)
t
$\frac{dT}{dt} = g(T) - \left(\frac{K_{max} \cdot C_p^{\gamma}}{KC_{50}^{\gamma} + C_p^{\gamma}}\right) \cdot T$
$g(T) = k_{ng} \cdot T \cdot (1 - T/T_{ss})$

Figure 7